ARTICLE

Check for updates

Journal of
Sensor Science and Technology

The Korean Sensors Society

Fluorescence-Based Optical Flow Sensor with Direction-Independent Response

Dongmin Seo[1], Jaemin Park[2], Seungmin Yoon[2], Sangwon Lee[2], Hansang Wi[2], Seonghoon Kang[2], Hojun Yoon[2], Sung-Hoon Byun[3], and Sangwoo Oh[3,+]

[1]*Department of Electrical and Electronic Engineering, Semyung University, 65 Semyung-ro, Jecheon 27136, Republic of Korea*
[2]*Department of Electrical Engineering, Semyung University, 65 Semyung-ro, Jecheon 27136, Republic of Korea*
[3]*Ocean and Maritime Digital Technology Research Division, Korea Research Institute of Ships and Ocean Engineering, 32 Yuseong-daero, Daejeon 34103, Republic of Korea*

Cite This: *J. Sens. Sci. Technol. Vol. 34, No. 6 (2025) 638-644*

https://doi.org/10.46670/JSST.2025.34.6.638

ABSTRACT: Non-contact flow-sensing technologies have attracted increasing attention in various fields, such as microfluidic control and underwater flow monitoring. In this study, an optical flow-sensing principle based on the fluorescence response of a phosphor-attached hollow pillar is proposed. The hollow structure of the ethylene propylene diene monomer pillar serves as an optical waveguide, delivering blue excitation light from an LED to a phosphor bead attached to the pillar tip, where red fluorescence is emitted and subsequently detected. Flow-induced deformation of the pillar causes a slight inclination of the phosphor, resulting in measurable variations in the detected fluorescence intensity. The fluorescence response was quantitatively analyzed under different flow rates (0–3000 mL/min) and directions (frontal and lateral) using three pillars with different outer diameters (Ø2.8, Ø3.8, and Ø4.8 mm). The results show a consistent decrease in the fluorescence intensity with an increasing flow rate and rapid recovery once the flow ceases. Smaller-diameter pillars exhibit higher sensitivity, and the overall response remains independent of the flow direction. These findings demonstrate that the proposed fluorescence-based optical sensor provides a simple and effective approach for multidirectional flow detection and can be applied to precise flow measurements in microfluidic and underwater environments.

KEYWORDS: *Fluorescence-based optical sensor, Flow detection, Non-contact sensing, Multidirectional flow sensing, EPDM pillar structure*

1. INTRODUCTION

Flow sensing plays a crucial role in a wide range of engineering and biological applications, including microfluidic control, underwater environmental monitoring, and environmental instrumentation [1-4]. Conventional flow sensors that rely on contact mechanisms, such as pressure-based, thermal, and turbine types, often suffer from issues such as signal interference, contamination, and reduced component durability owing to direct contact with the target fluid [5-8]. Consequently, non-contact optical sensors have attracted increasing attention because of their high sensitivity, fast response, and tolerance to electromagnetic interference, resulting in various studies being conducted [9,10].

Among the different optical sensing approaches, fluorescence-based detection exhibits particularly high sensitivity [11,12]. Fluorescence signals respond sensitively to changes in the optical path, emission direction, and surroundings, making them suitable for the quantitative detection of subtle physical shifts. Based on these characteristics, fluorescence-based sensing techniques have been widely applied in various fields, including concentration measurements, temperature monitoring, and particle tracking analysis [13-17]. However, few studies have utilized fluorescence signals to detect the stream velocity or structural deformation induced by the flow quantitatively. In particular, systematic analyses of the fluorescence response under varying flow directions have seldom been reported.

In previous studies, an ethylene propylene diene monomer (EPDM) hollow pillar structure coated with phosphor was utilized to analyze changes in the external force-induced fluorescence intensity, demonstrating the capability of a non-

[+]Corresponding author: hope2ryan@gmail.com
Received : Oct. 15, 2025, Revised : Oct. 23, 2025, Accepted : Oct. 30, 2025

This is an Open Access article distributed under the terms of the Creative Commons Attribution Non-Commercial License (https://creativecommons.org/licenses/by-nc/3.0/) which permits unrestricted non-commercial use, distribution, and reproduction in any medium, provided the original work is properly cited.

contact flow-detection approach based on fluorescence response [18,19]. The fluorescence intensity varied linearly with the tilting degree of the phosphor attached to the upper surface of the pillar, and the sensitivity differences depending on the pillar diameter and shape were experimentally verified. However, these experiments were limited to the static conditions of the external force using a force gauge sensor, and the fluorescence response characteristics under real flow fields, as well as the correlation between the flux and signals, were not fully clarified.

In this study, a flow-controllable chamber was designed to investigate the changes in the fluorescence response under real fluid flow conditions to address these limitations. Using this methodology, the mechanical deformation of the pillar and corresponding fluorescence intensity changes were quantitatively analyzed as a function of the stream velocity, thereby validating the proposed fluorescence-based flow-sensing principle in real flow environments. In particular, both frontal and lateral flow directions were applied to assess the consistency of the fluorescence response under multidirectional conditions, confirming the feasibility of fluorescence-based optical sensors for multidirectional flow detection.

In this paper, the design of the proposed fluorescence-based flow detection structure is presented, followed by experimental validation. Section 2 describes the configuration of the experimental setup, optical system, and image analysis methodology. Section 3 analyzes the fluorescence response characteristics with respect to variations in the pillar diameter and flow direction (frontal/lateral). Finally, Section 4 summarizes the key findings of the study and discusses the potential applicability of the proposed sensor structure for real-time multidirectional flow detection.

2. METHODS

2.1 Fabrication of Phosphor-Attached Pillars

2.1.1 Pillar Structure and Specifications

Fig. 1 shows the structure and key specifications of the phosphor-attached pillars fabricated in this study. The pillars were made of EPDM rubber, with a fixed length of 15.0 mm and an inner diameter of 1.8 mm. The outer diameter was varied to 2.8, 3.8, and 4.8 mm for three different configurations, hereinafter referred to as the Ø2.8, Ø3.8, and Ø4.8 pillars, respectively.

A hollow core with a diameter of 1.8 mm was formed at the center of each pillar to function as an optical waveguide. In this structure, the excitation light exposed from a blue LED (470 ± 10 nm) was guided through the hollow channel to the phosphor on the upper surface of the pillar, and the red fluorescence emitted from the excited phosphor was then transmitted back through the same optical path to the camera. This optical path design minimizes scattering losses towards the filler exterior and enables stable detection of changes in fluorescence intensity.

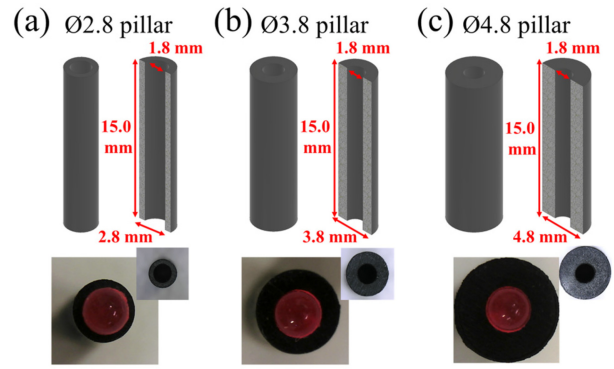

Fig. 1. Structure and dimensions of the phosphor-attached pillars. Each pillar was classified according to its outer diameter, namely (a) Ø2.8, (b) Ø3.8, and (c) Ø4.8, while maintaining the same height of 15.0 mm and inner diameter of 1.8 mm. The bottom images show the hollow structure observed from the top of each pillar and actual photographs of the phosphor attached to the upper surface.

2.1.2 Phosphor Attachment Process

A phosphor was attached to the upper surface of the pillar to visualize fluorescence responses under varying flow conditions. The phosphor consisted of a spherical bead made of soda–lime glass (HCMS-P-SLGS-FMR, Ø2 mm, Cospheric, Goleta, CA, USA) coated with a red fluorescent material. The excitation and emission wavelengths of the phosphor were 575 and 607 nm, respectively, and the phosphor could be effectively excited by the 470 nm blue LED source owing to its broad absorption characteristics.

The phosphor was attached to the upper central surface of the pillar using an adhesive to ensure alignment between the optical axis of the hollow channel and center of the phosphor. The attached phosphor was cured at room temperature for more than 24 h to ensure bonding stability. An instant-curing adhesive (Loctite 406, Henkel Loctite Co., Ltd., Shandong, China) with significant adhesion to rubber was used for this process.

2.2 Configuration of Flow Test System and Measurement Method

2.2.1 Experimental Setup

Fig. 2 shows a schematic of the experimental setup used to evaluate the flow-response characteristics of the phosphor-

ⓒ The Korean Sensors Society

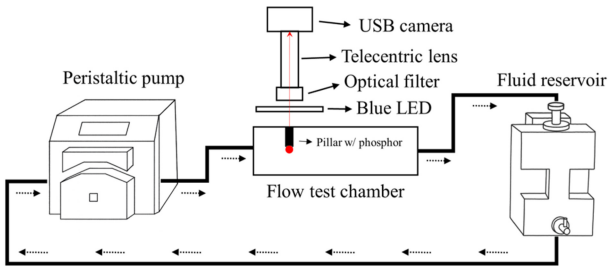

Fig. 2. Schematic of the experimental setup for evaluating the flow-response characteristics of the phosphor-attached pillar.

attached pillar. The system consisted of a peristaltic pump, a flow test chamber, a fluid reservoir, and an optical observation system.

A peristaltic pump (Masterflex I/P® Digital Process Drive, Masterflex, Vernon Hills, IL, USA) coupled with Puri-Flex® Tubing I/P 26 (Masterflex, USA) was employed for fluid circulation. This pump system was used to circulate the fluid, and the flow rate was controlled within the range of 0–3000 mL/min, considering the pump capability and inner diameter of the tubing.

Triple-distilled water was used as the circulating fluid to minimize optical interference caused by impurities. The pump was carefully configured such that the fluid flowed in the direction indicated by the dashed arrows, aligning the inflow nozzle center with the phosphor center to ensure that the flow penetrated the phosphor frontally. The phosphor-attached pillar was vertically fixed inside the flow test chamber, and an observation window was installed at the top to enable non-contact optical measurement of fluorescence responses.

The flow test chamber was constructed as an internal rectangular structure with dimensions of 130.0 mm × 73.5 mm × 53.7 mm. Inlets and outlets were configured on opposite sides of the chamber, allowing division of the flow conditions by the inflow direction. The frontal flow condition refers to the fluid entering through a nozzle on the short side (73.5 mm direction) and impinging the front pillar surface; in contrast, the lateral flow condition corresponds to fluid entering from a nozzle on the long side (130.0 mm direction), interacting with the pillar from a different direction. The distance between the nozzle and pillar, as well as the phosphor position, were maintained identical in both conditions so that the internal flow distribution was changed solely by the length difference of the flow path from the inlet to outlet.

All experiments were conducted using the same top-view observation, allowing for direct comparison of the fluorescence response characteristics under identical observation directions but different flow directions.

2.2.2 Optical Observation System

An optical observation system was constructed to measure the fluorescence response characteristics of the phosphor-attached pillars in a non-contact manner.

A USB camera (acA2440-75um, Basler, Ahrensburg, Germany) was used for fluorescence signal detection. The camera was equipped with a telecentric lens (CompactTL™, Edmund Optics, Barrington, NJ, USA) and a band-pass filter (center 607 nm, FWHM 36 nm; Edmund Optics, Barrington, NJ, USA). The telecentric lens minimized the focus dispersion caused by variations in the phosphor depth, reducing distortion of the observed signal, whereas the band-pass filter blocked the excitation light from the LED (470 ± 10 nm) while selectively transmitting only the fluorescence signal emitted from the phosphor (607 ± 36 nm).

A ring-type LED light source (SpecBright™; ProPhotonix, Boston, MA, USA) was used as the excitation source. The LED was positioned vertically on the upper surface of the chamber to deliver the excitation light uniformly along the inner channels of the pillars. The optical axis of the LED was aligned with the central axis of the pillar to maintain a consistent excitation intensity of the light impinging on the phosphor. The pillar was fixed onto a glass slide, and the red fluorescence emitted from the phosphor was passed through the band-pass filter to be captured by the camera.

2.2.3 Image Acquisition and Measurement Procedure

The optical system parameters for the fluorescence response measurements were maintained identical throughout all experiments. The LED light source was operated in the constant-current mode (24 V, 350 mA), and the camera settings were fixed at a gain of 36, an exposure time of 70 ms, a frame rate of 10 fps, and gamma of 0.8. These parameters were selected to prevent fluorescence signal saturation while ensuring a sufficient signal-to-noise ratio.

The flow experiments started with recording the reference fluorescence intensity under a flow rate of 0 mL/min, followed by gradually increasing the flow rate. Fluorescence signals were acquired at 1000, 2000, and 3000 mL/min. Data were collected for 20 s from each flow rate, and the experiments were repeated under identical conditions for all three pillar types (Ø2.8, Ø3.8, and Ø4.8).

The acquired fluorescence images were processed using the ImageJ software (version 1.54k, National Institutes of Health, USA). The phosphor region was designated as the region of interest (ROI), and both the mean grayscale intensity and maximum intensity of each frame were calculated. To avoid signal saturation, the system was adjusted so that the maximum pixel brightness did not exceed 255 on an 8-bit scale. Using these calibrated conditions, the characteristics of

ⓒ The Korean Sensors Society

the fluorescence intensity response to varying flow velocities were quantitatively analyzed and the differences in the responses among the pillar geometries were systematically compared.

3. RESULTS AND DISCUSSION

3.1 Fluorescence Image-Based Flow-Response Analysis

3.1.1 Fluorescence Image Analysis Method

Fig. 3 shows the quantitative analysis results of the brightness variations in the fluorescence images.

Fig. 3(a) shows representative fluorescence images obtained at flow rates of 0, 1000, 2000, and 3000 mL/min. The closed yellow curve in each image indicates the ROI, which was consistently defined along the projected circumference of the phosphor. By maintaining a constant ROI, the analysis results were prevented from being influenced by focus shifts or differences in the observation field. The images were acquired in an 8-bit format, and the maximum pixel value was adjusted so as not to exceed 255 to prevent fluorescence signal saturation.

(a)

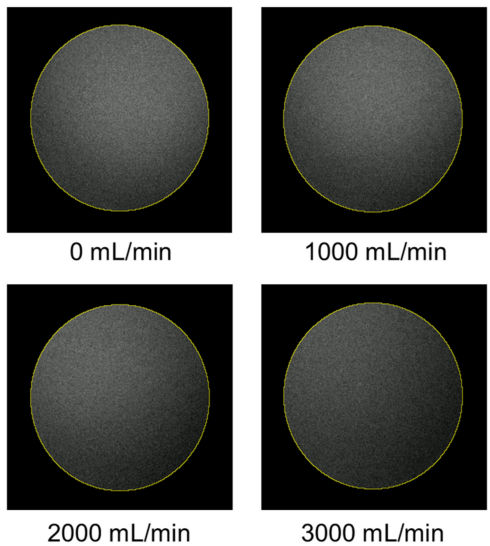

(b)

Flow rate (mL/min)	0	1000	2000	3000
Area (pixels)	30,525	30,525	30,525	30,525
Mean (a.u.)	80.196	75.494	67.004	56.702
Max (a.u.)	138	135	131	119

Fig. 3. Quantitative analysis of fluorescence intensity under varying flow conditions. (a) Representative fluorescence images acquired at flow rates of 0, 1000, 2000, and 3000 mL/min. The yellow circular mark in each image indicates the region of interest (ROI) used for analysis. (b) Mean and maximum intensity values measured from the ROI at each flow rate.

Fig. 3(b) presents the quantitative results obtained from the ROI specified in Fig. 3(a). The ROI area was fixed at 30,525 pixels, and as the flow rate increased, the mean fluorescence intensity (a.u.) decreased as 80.196 → 75.494 → 67.004 → 56.702, while the maximum intensity (a.u.) gradually reduced as 138 → 135 → 131 → 119. At 3000 mL/min, the mean and maximum intensities were reduced by 29.3% and 13.8%, respectively, compared with the initial condition of 0 mL/min. This trend was attributed to the slight tilting of the pillar top at higher flow velocities, which caused a portion of the emitted light to deviate from the detection axis. This implies that flow-induced changes in the emission path directly influence the detection intensity, demonstrating that micro-deformation of the pillar can be detected via fluorescence signal variations.

3.1.2 Fluorescence Response According to Pillar Diameter

Fig. 4 shows a comparison of the fluorescence response characteristics with respect to the outer diameters of the pillars. All experiments were performed under identical optical conditions (LED: 24 V, exposure: 70 ms, gain: 36, gamma: 0.8, and frame rate: 10 fps), and the mean intensity within the ROI was calculated for each condition.

Fig. 4(a) shows the results under frontal flow conditions. As the flow rate increased, the fluorescence intensities of all three pillars gradually decreased. In particular, the Ø2.8 pillar showed the largest attenuation, with a decrease of approximately 30% at 3000 mL/min compared with the initial state. This behavior indicates that smaller-diameter pillars experience larger deformation under the same flow, leading to a greater deviation in the emitted light from the detection axis owing to tilting of the phosphor. In contrast, the Ø4.8 pillar with relatively higher stiffness exhibited smaller variations in fluorescence intensity.

Fig. 4(b) shows the results under lateral flow conditions. Despite the identical experimental setup and flow rates to those used for frontal flow, the degree of fluorescence attenuation was even greater. At a flow rate of 3000 mL/min, the mean intensity decreased to approximately 45 a.u., indicating that a stronger fluidic force was transmitted during lateral flow according to the different internal flow distributions and relative distances to the walls. Consequently, greater pillar deformation occurred, leading to further deviation of the emission path and a larger decrease in the fluorescence intensity.

These results confirm that smaller pillar diameters yield higher flow-detection sensitivity and that the fluorescence intensity consistently decreases, regardless of changes in flow

ⓒ The Korean Sensors Society

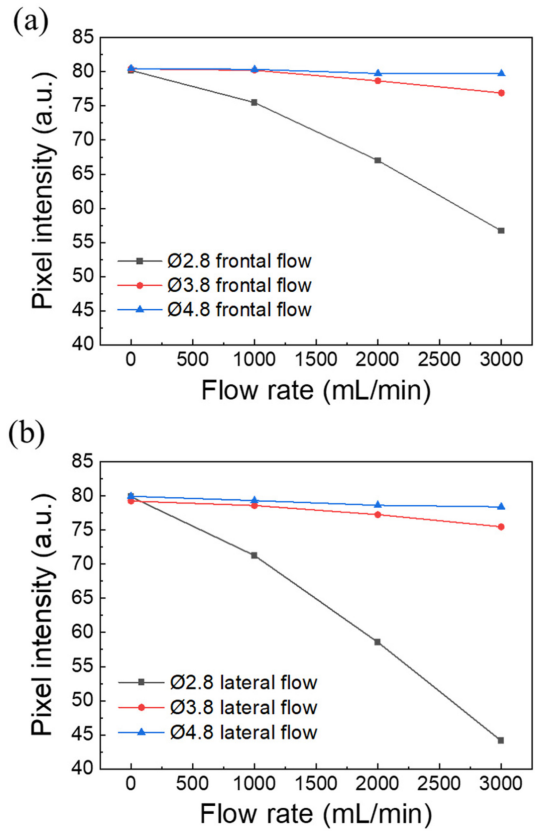

Fig. 4. Comparison of fluorescence response according to pillar diameter (Ø2.8, Ø3.8, and Ø4.8 mm). (a) Fluorescence intensity variation under frontal flow conditions. (b) Fluorescence intensity variation under lateral flow conditions.

direction. Therefore, the pillar diameter was identified as a key design parameter that directly affects the sensitivity of fluorescence-based flow detection.

3.2 Fluorescence Response Characteristics According to Flow Direction

Figs. 5 and 6 show the frame-by-frame variations in the fluorescence response signals under frontal and lateral flow conditions, respectively. All experiments were performed under identical conditions (LED: 24 V, exposure: 70 ms, gain: 36, gamma: 0.8, and frame rate: 10 fps) and at the same flow rates (0, 1000, 2000, and 3000 mL/min). In each graph, the x-axis represents the frame number and the y-axis represents the mean brightness intensity within the ROI. Data were collected for approximately 20 s at 10 fps, allowing for the temporal observation of fluorescence intensity changes during flow initiation and shutoff.

Figs. 5(a)–(c) depict the fluorescence signal variations for each pillar diameter under frontal flow conditions. Upon flow initiation, the fluorescence intensity immediately decreased for

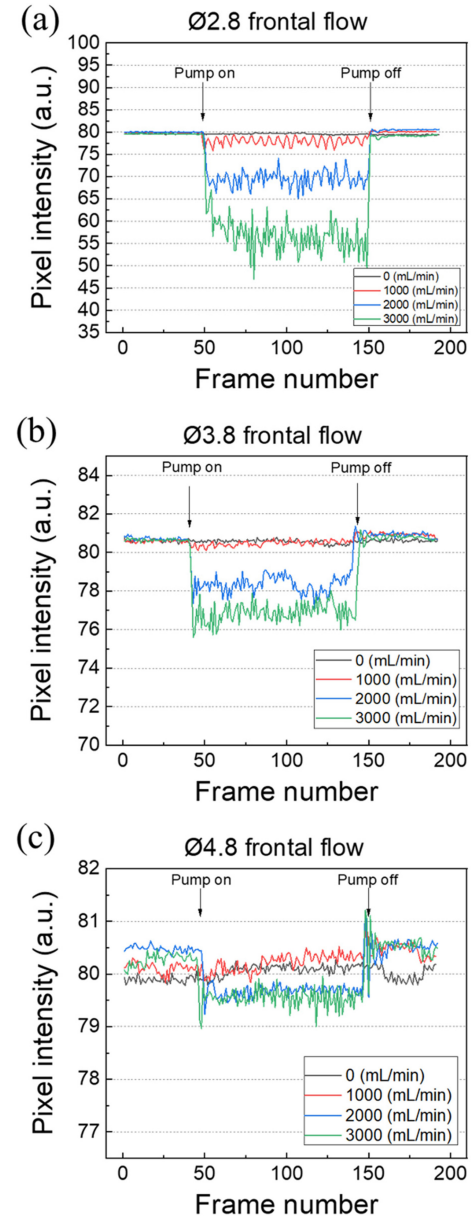

Fig. 5. Frame-by-frame fluorescence response according to the pillar diameter under frontal flow conditions. (a) Ø2.8, (b) Ø3.8, and (c) Ø4.8 pillars showing variations in fluorescence intensity.

all pillars, with a consistent tendency of greater attenuation observed at higher flow rates. The Ø2.8 pillar (Fig. 5(a)) exhibited the largest degree of intensity reduction, showing a decrease of approximately 40% in the mean brightness at 3000 mL/min. The signal responded instantaneously to flow initiation and recovered rapidly after flow shutoff, confirming high responsiveness and repeatability. The Ø3.8 pillar (Fig. 5(b)) displayed more gradual attenuation with a stable vibration component of the signal. In contrast, the Ø4.8 pillar (Fig. 5(c)) exhibited an extremely narrow brightness variation of less than 1 a.u., resulting in difficult detection of actual flow

ⓒ The Korean Sensors Society

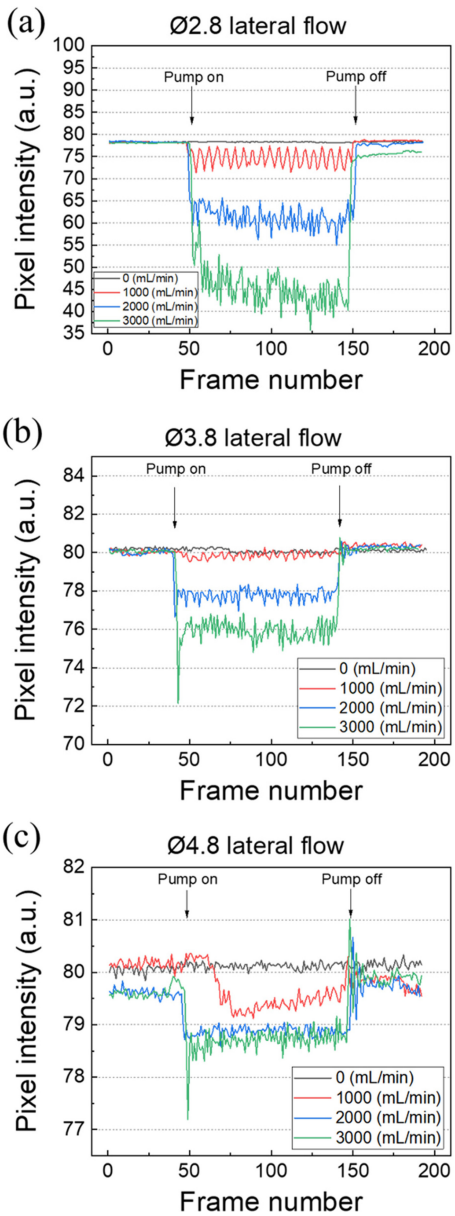

Fig. 6. Frame-by-frame fluorescence response according to the pillar diameter under lateral flow conditions. (a) Ø2.8, (b) Ø3.8, and (c) Ø4.8 pillars showing variations in fluorescence intensity.

changes. This behavior is attributed to the increased stiffness of the pillar, which led to reduced deformation and minimal alteration of the fluorescence emission path. Nevertheless, the mean brightness fluctuation remained below ±0.25 a.u. (approximately 0.6% of the average) during the non-flow intervals, indicating that the measured signal remained stable. The apparently large fluctuations in the Ø4.8 pillar signal were a visual effect arising from differences in the vertical scale (y-axis). In contrast, the more flexible Ø2.8 and Ø3.8 pillars exhibited noticeable periodic oscillations in fluorescence intensity that corresponded to the pulsation of the peristaltic pump, demonstrating fluorescence signals capable of responding instantaneously to minimal flow variations. This finding indicates the potential of the system for implementation as a real-time flow-rate-sensing platform.

Figs. 6(a)–(c) show the fluorescence signal variations as a function of the pillar diameter under lateral flow conditions. The experimental parameters were the same as those under frontal flow conditions and only the flow direction was altered. Similar to the frontal flow case, the fluorescence intensity decreased immediately upon flow initiation, and the degree of attenuation increased with the flow rate for all pillars. However, the overall degree of fluorescence signal reduction was larger than that observed under frontal flow, and the Ø2.8 pillar (Fig. 6(a)) exhibited a more noticeable decrease of approximately 50% at 3000 mL/min compared with the initial intensity. This could be attributed to the flow distribution within the chamber and relative distance to the walls, which caused a stronger fluidic force on the pillar. The Ø3.8 pillar (Fig. 6(b)) showed similar response characteristics to those under frontal flow, but with more pronounced attenuation with flow rate variations. Conversely, the Ø4.8 pillar (Fig. 6(c)) still exhibited minimal variations, with signal changes approaching the noise level.

These findings demonstrate that the fluorescence-based flow-sensing system operates reliably, regardless of the flow direction. In both the frontal and lateral flow cases, the fluorescence intensity consistently decreased upon flow initiation and recovered immediately after shutoff.

Therefore, the proposed fluorescence sensor structure maintains sensing performance under varying flow directions, experimentally verifying its multidirectional (direction-independent) flow-response capability.

4. CONCLUSION

In this study, a fluorescence response-based optical flow sensor employing a phosphor-attached hollow pillar structure was proposed, and its response characteristics were experimentally validated under real flow conditions. The pillar was fabricated using EPDM material, and the hollow core allowed the excitation light from a blue LED to be transmitted to the phosphor, while the emitted red fluorescence was guided back through the same optical path for detection. This configuration enabled the quantitative, non-contact measurement of fluorescence intensity variations resulting from minute tilting of the phosphor at the upper surface of the pillars.

The comparative analyses performed for all three pillars with different diameters (Ø2.8, Ø3.8, and Ø4.8 mm) under both frontal and lateral flow conditions demonstrated that the

ⓒ The Korean Sensors Society

fluorescence intensity consistently decreased with an increasing flow rate and immediately recovered when the flow was stopped. In particular, the Ø2.8 pillar exhibited the largest attenuation, confirming that smaller diameters yield higher deformation sensitivity. Moreover, the consistent attenuation and recovery characteristics in different flow directions verified the multidirectional flow responsivity of the proposed fluorescence-based sensor. Based on these findings, the fluorescence response-based non-contact optical sensor demonstrates high sensitivity and fast response in flow environments.

Further research will focus on optimizing the pillar material, geometry, and phosphor configuration to enhance the sensitivity and linearity, ultimately verifying its applicability to a compact, low-power flow-sensing module for practical applications.

CRediT Authorship Contribution Statement

Dongmin Seo: Conceptualization, Formal analysis, Investigation, Methodology, Project administration, Validation, Visualization, Writing – original draft, Writing – review & editing. **Jaemin Park, Seungmin Yoon, Sangwon Lee, Hansang Wi, Seonghoon Kang, and Hojun Yoon:** Data curation, Methodology, Software, Visualization. **Sung-Hoon Byun:** Funding acquisition, Project administration, Resources. **Sangwoo Oh:** Conceptualization, Investigation, Methodology, Project administration, Supervision, Writing – review & editing.

Declaration of Competing Interest

The authors declare that they have no known competing financial interests or personal relationships that could have appeared to influence the work reported in this paper.

Acknowledgements

This research was supported by a grant from Endowment Project of "Development of Smart Sensor Technology for Underwater Environment Monitoring" funded by Korea Research Institute of Ships and Ocean engineering (PES5550). This work was also supported by the Regional Innovation System & Education (RISE) program through the Chungbuk Regional Innovation System & Education Center, funded by the Ministry of Education (MOE) and the Chungcheongbuk-do, Republic of Korea (2025-RISE-11-008-01).

REFERENCES

[1] L. Zhang, Z. Hang, H. Hu, Bio-inspired artificial hair flow sensors: a comprehensive review of design, fabrication, enhancements, and applications, Microsyst. Nanoeng. 11 (2025) 88.

[2] M.A. Nour, M.M. Hussain, A review of the real-time monitoring of fluid-properties in tubular architectures for industrial applications, Sensors 20 (2020) 3907.

[3] J. Kim, Development of artificial lateral line sensor for flow velocity and angle measurements, J. Sens. Sci. Technol. 30 (2021) 30–35.

[4] M.R. Arshad, Recent advancement in sensor technology for underwater applications, Indian J. Mar. Sci. 38 (2009) 267–273.

[5] J.C. Choi, J.K. Lee, S.H. Kong, Fabrication and characteristics of micro-electro-mechanical-system-based gas flow sensor, J. Sens. Sci. Technol. 20 (2011) 363–367.

[6] H. Lundström, Investigation of heat transfer from thin wires in air and a new method for temperature correction of hot-wire anemometers, Exp. Therm. Fluid Sci. 128 (2021) 110403.

[7] Bunyamin, N.L. Husni, H. Basri, I. Yani, Challenges in turbine flow metering system: an overview, J. Phys. Conf. Ser. 1198 (2019) 042010.

[8] R.E. Oosterbroek, T.S.J. Lammerink, J.W. Berenschot, G.J.M. Krijnen, M.C. Elwenspoek, A. van den Berg, A micromachined pressure/flow-sensor, Sens. Actuators A Phys. 77 (1999) 167–177.

[9] S. Gao, H. Ma, A study on structure improvement scheme of electromagnetic flow sensor for slurry flow measurement, Meas. Control 55 (2022) 519–534.

[10] K. Tezuka, M. Mori, T. Suzuki, T. Kanamine, Ultrasonic pulse-Doppler flow meter application for hydraulic power plants, Flow Meas. Instrum. 19 (2008) 155–162.

[11] X. Wang, R. Wang, S. Du, J. Chen, S. Tan, Flow visualization and mixing quantification in a rod bundle using laser induced fluorescence, Nucl. Eng. Des. 305 (2016) 1–8.

[12] K. Girigoswami, N. Akhtar, Nanobiosensors and fluorescence based biosensors: an overview, Int. J. Nano Dimens. 10 (2019) 1–17.

[13] D. Sinton, Microscale flow visualization, Microfluid. Nanofluid. 1 (2004) 2–21.

[14] T. Zhang, L. Liu, H. Yang, Y. Wang, D. Chen, J. Wang, et al., Microfluidic quantitative flow cytometer with light modulation, IEEE Sens. J. 22 (2022) 3009–3016.

[15] P. Löw, B. Kim, N. Takama, C. Bergaud, High-spatial-resolution surface-temperature mapping using fluorescent thermometry, Small 4 (2008) 908–914.

[16] F. Tauro, G. Mocio, E. Rapiti, S. Grimaldi, M. Porfiri, Assessment of fluorescent particles for surface flow analysis, Sensors 12 (2012) 15827–15840.

[17] F. Tauro, Particle tracers and image analysis for surface flow observations, Wiley Interdiscip. Rev. Water 3 (2016) 25–39.

[18] D. Seo, S. Oh, S.-H. Byun, Image analysis for the simultaneous measurement of underwater flow velocity and direction, J. Sens. Sci. Technol. 32 (2023) 307–312.

[19] D. Seo, S. Yoon, J. Park, S. Lee, S. Han, S.-H. Byun, et al., Optical flow sensor with fluorescent-conjugated hyperelastic pillar: a biomimetic approach, Biomimetics 9 (2024) 721.

ⓒ The Korean Sensors Society